Effect of Trailing-Edge Bevel Angle on the Sound Generation of a Flat Plate

Alper Celik*, Luke Bowen† and Mahdi Azarpeyvand ‡
University of Bristol, Bristol,UK, BS8 1TR

An experimental study was conducted to investigate the effect of the trailing-edge bevel angle on the noise radiated from the trailing-edge and the corresponding hydrodynamic field. The Reynolds number based on the length of the adjustable bevel part length was $Re = 1.4\mathbf{x}10^5$. Results are presented for bevel angles $0^\circ < \alpha < 28^\circ$. The hydrodynamic field is characterized by steady and unsteady pressure measurements and hot-wire measurements. Radiated noise from the trailing-edge was determined with a beamforming array. The results demonstrate that the increase in the bevel angle increases the radiated noise up to $\alpha = 8^\circ$ and the far-field noise level starts decreasing beyond the bevel angle of $\alpha = 8^\circ$. The corresponding hydrodynamic field on the beveled part of the trailing-edge displays an accelerated flow region with an accompanied increase in pressure coefficient values. In general, the energy spectra of the unsteady surface pressure fluctuation results indicates a slight broadband energy increase as the bevel angle increases for an attached flow. Moreover, the velocity-pressure coherence analysis reveals a significant reduction for the increased bevel angle which may be related to reduced size of the coherent structures indicated by the stream-wise coherence analysis.

I. Nomenclature

C_p	=	non-dimensional pressure coefficient
C_{prms}	=	non-dimensional pressure root-mean square value
f	=	frequency (Hz)
i, j	=	location indices
p	=	pressure (Pa)
p'	=	pressure fluctuation (Pa)
p_{ref}	=	reference pressure (2×10^{-5} Pa)
l	=	length of the adjustable trailing-edge (m)
Re	=	reynolds number
$R_{p'_i p'_i}$	=	auto-correlation of pressure fluctuation at microphone i
$R_{p_{i'} p_{j'}}$	=	cross-correlation of pressure fluctuation between microphones i and j
U_∞	=	free-stream velocity (m/s)
α	=	trailing-edge bevel angle (°)
ϕ_{pp}	=	power spectral density of the pressure fluctuation (dB/Hz)
PSD	=	power Spectral Density (dB/Hz)
$\gamma^2_{p'_i p'_j}$	=	wall pressure coherence between two pressure transducers
$\gamma^2_{p'_i u_i}$	=	coherence between pressure transducer and velocity
x, y, z	=	global coordinates based at the trailing edge
x', y'	=	local coordinate system
ξ	=	distance between two transducers in x or z direction (m)

*Post-Doctoral Research Associate, Mechanical Engineering, alper.celik@bristol.ac.uk
†PhD. Student, Mechanical Engineering, luke.bowen@bristol.ac.uk
‡Professor of Aerodynamics and Aeroacoustics, Mechanical Engineering, m.azarpeyvand@bristol.ac.uk

II. Introduction

The noise generated by the flow past a trailing-edge has been in the scope for many decades due to its extensive application area. It is encountered in every day life and whether it be the ever increasing reliance on air travel, or the growth of wind turbines in energy production schemes, noise pollution has evoked an increased awareness. Reduction of noise pollution is becoming ever important and research is focusing on decreasing the noise levels of these key instruments of modern life. An understanding of the fundamental mechanisms that leads to noise generation is one of the key aspects for noise attenuation studies and this can start with simple geometries. Beveled trailing-edge geometries are of extensive application and found in many areas of not only aviation but engineering and modern technology. Deflected blades or flaps on wings, as well as automotive vehicle geometry are examples of this but generally a structure with a slanted edge will fall into this category of noise generation.

The main self-noise generation mechanisms identified by Brooks *et al.* [1] are all shown to contribute to the noise generated by an airfoil, however turbulent boundary layer interaction with the trailing edge is the main source generating the broadband noise in most applications. The understanding of the mechanisms has been well explored [1–4], and with assumptions, comparisons are drawn between the noise generated at trailing edge and various physical quantities for low mach number flows. These include; surface pressure fluctuation, span-wise eddy length scale, two-point velocity cross-correlation and convection velocity. A reduction in radiated noise to the far field should be achieved by reducing any of these quantities, or in any combination. For this reason, there have been many studies in noise abatement at the trailing edge with multiple methods of both active [5, 6] and passive [7–9] flow control to try to suppress the noise generated at the trailing edge by reducing the stated parameters. However, assumptions within the presented solutions make this more difficult because an idealized trailing edge is not practical for most geometries, or convected eddies are not affected by the presence of a trailing edge. Due to the stated reason an approach of tentation is generally adopted for flow control techniques for noise reduction at the trailing edge. Although measurable noise reduction has been observed in many cases, be that serrations [8–10], or porous materials [7], to optimise noise reduction further understanding of the fundamental physical mechanisms of noise generation is required. To achieve this, the noise generation mechanisms must be understood and their relation to the surface pressure behaviour and flow structures, which has produced a number of studies on airfoils [11, 12], high lift configurations [13–15], flat plates [16, 17], as well as cavities [18, 19].

A beveled trailing-edge geometry can exacerbate turbulent boundary layer trailing edge noise generation and one of the original works on this geometry was an extensive study by Blake [20, 21], studying the flow field and associated noise generation. The study considers a wide range of geometries, not only the beveled trailing edge but blunt and knuckled shapes too and concluded that the boundary layer behaviour and the flow around the trailing edge may limit the noise prediction. Howe followed up this work with a two part study [22, 23], reporting that the hydro-acoustic sources associated with lift fluctuations and the finite thickness of the airfoil are the two main mechanisms that contribute to beveled trailing edge noise. High frequency noise radiation is caused by the beveled surface for an attached flow, and once separated the noise emission from the trailing edge is exponentially decreases as eddies in the shear layer do not interact with the trailing edge. The specific flow structures that are introduced due to the presence of the bevelled trailing edge were the subject of recent experimental and numerical studies [24–27] linking them to the noise generation for improvement of prediction models. Guan *et al.* [27, 28] studied the flow structures over the beveled trailing edge and in the wake to generate more understanding between the geometry, the unsteady surface pressure fluctuations and structures in the wake.

The aim of the present study is to continue the development of the fundamental understanding of the noise generation mechanisms and generated noise for a beveled trailing-edge, and by doing so, form a basis to understand more complex noise generation mechanisms including, but not limited to, trailing-edge serrations, cavities with beveled edges and flaps. A flat plate test rig with an adjustable trailing edge section was used to investigate the effect of bevel angle on the hydrodynamic field and trailing-edge noise radiation mechanisms.

III. Experimental Set-Up

To study the effect of the trailing-edge bevel angle on noise generation, a flat plate rig with an adjustable trailing edge is used. It was designed and manufactured in-house at the university of Bristol and is 900 mm in length. Figure 1 depicts the experimental set up, the flat plate and adjustable trailing edge and measurement locations. The flat plate was instrumented to effectively capture the characteristics of the flow with 12 steady pressure taps for hydrodynamic field measurement, and 12 unsteady surface pressure taps for near-field noise measurements. The flat plate rig was tested in the anechoic wind tunnel facility at the University of Bristol, which is an closed circuit, open-jet wind tunnel. It has a nozzle height of 775 mm and width of 500 mm which delivers a steady flow with a freestream turbulence intensity of

less than 0.2% [29]. The nozzle opens out into a test chamber that is acoustically lined, 6.7 m in length, 4.0 m in width and 3.3 m in height and anechoic down to 160 Hz. The flat plate was mounted on the lip of the nozzle exit and the flow was bound by side plates which were 250 mm longer than the flat plate. The flow was tripped at 20% of the length to ensure the presence of a fully turbulent boundary layer over the flat plate. The last 100 mm of the flat plate was designed with a hinge to allow for different bevel angles, α, to be adjusted over the range $0° < \alpha < 28°$. The free-stream velocity for the test was $U_\infty = 20m/s$ which corresponds to adjustable bevel part length Reynolds number of Re = 1.4 x 10^5.

The unsteady surface pressure measurements were performed using in-situ microphone instrumentation which allow for the detailed capture of surface pressure fluctuations. A total of 12 Knowles FG-23329-P07 miniature pressure transducers were used and are 2.6mm in diameter with a circular sensing area of 0.8mm. The flat plate was machined to have a 0.4mm pinhole mask to avoid pressure attenuation at high frequencies and the locations are presented in Fig. 1. The data was collected for 16 seconds at a sampling frequency of 2^{16} Hz. All the microphones were calibrated for both phase and magnitude which references a GRAS 40PL microphone, which itself is calibrated using a GRAS 42AA pistonphone calibrator. The near-field data was acquired by using four National Instrument PXI-e4499 cards and were driven by a Matlab script. Steady pressure measurements were carried out using two 32 channel Chell MicroDAQ pressure scanners at a sampling frequency of 1000 Hz for 16 seconds and have a full-scale accuracy of 0.05%. The averaged results were used to present non-dimensional pressure coefficient C_p and C_{prms}.

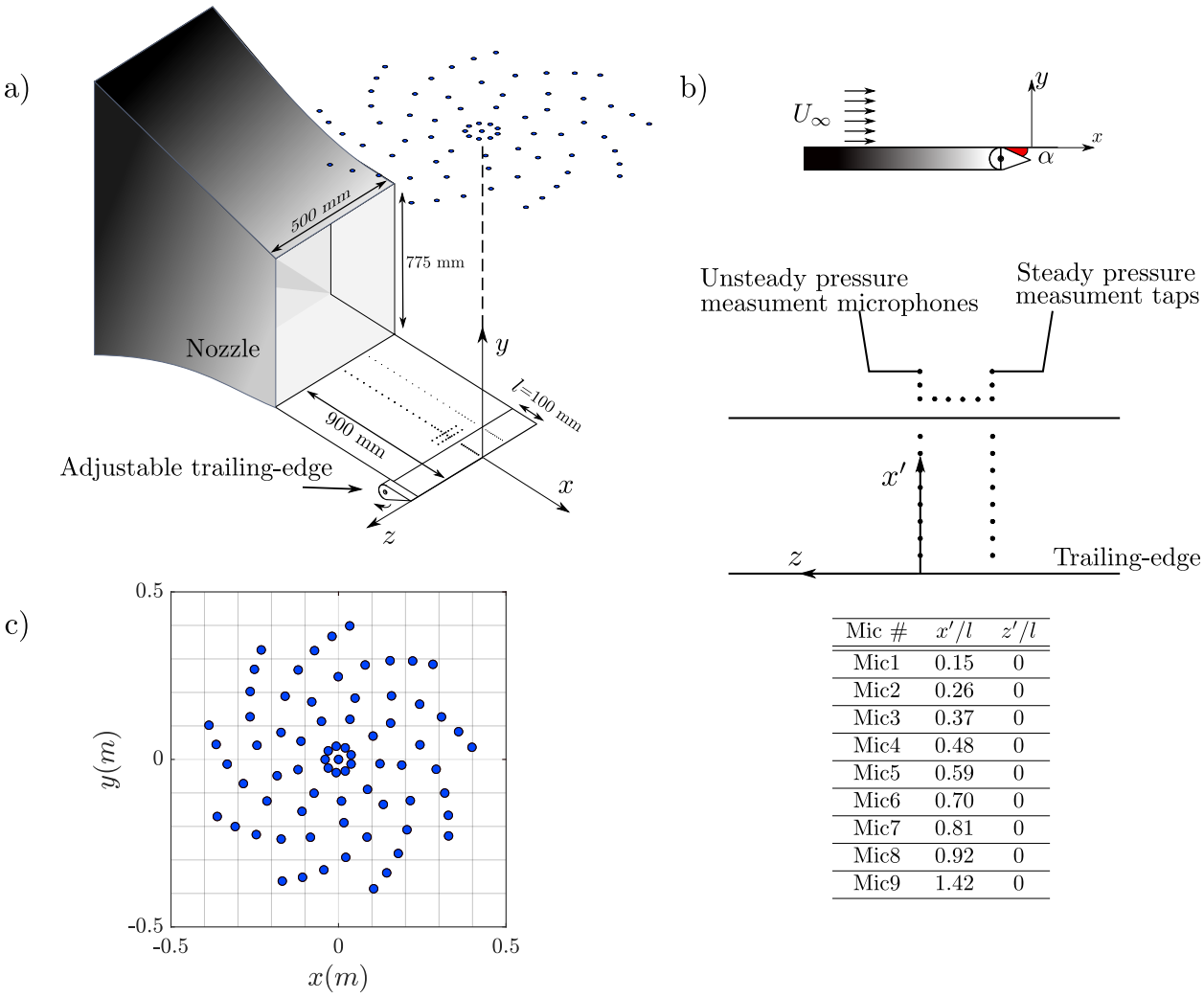

Mic #	x'/l	z'/l
Mic1	0.15	0
Mic2	0.26	0
Mic3	0.37	0
Mic4	0.48	0
Mic5	0.59	0
Mic6	0.70	0
Mic7	0.81	0
Mic8	0.92	0
Mic9	1.42	0

Fig. 1 Schematics of the beveled flat plate rig, a) the experimental set up with the contraction nozzle and beamforming array location, b) location of unsteady and steady pressure measurements, c) the arrangement of the microphones on the beamforming array.

The far-field measurements were conducted by the in-house built beamforming array [30] which consists of 73 Panasonic WM-61A microphones and located 1.2 meters above the test rig. Figure 1 shows the arrangement of the array which has 9 spiral arms, each with 8 microphones. The trailing edge of the flat plate is aligned with the centre of the beamforming array and the data was collected for 120 seconds at a sampling frequency of 2^{15} Hz.

Constant Temperature Hot-wire Anemometry measurements were carried out over the surface and in the wake of the flat plate to characterise the mean velocity field and turbulent structures in the flow. Velocity measurements on the flat plate were conducted using a 55P15 boundary layer probe and wake measurements with a 55P51 cross-wire probe. The probes were calibrated by using the Dantec 54H10 type calibrator and the 55P51 cross-wire probe was calibrated for yaw angles between -40° and 40°. The probes were operated with a Dantec Streamline Pro system with CTA 91C10 modules, and the measurements were sampled at a frequency of 2^{15} Hz for 60 seconds using a National Instruments PXIe-4499 modules mounted in a National Instruments PXIe-1062Q chassis. The probes location and traverse movements were controlled with a two-axis ThorLabs LTS300M traverse system.

IV. Results & Discussions

The hydrodynamic phenomena generated by the flow field and subsequent far field noise radiation are presented for a beveled trailing edge subjected to a one-sided flow. The hydrodynamic field around the geometry is reported, comparing a straight trailing edge to various selected angles of the bevel, characterising the steady pressure coefficient and unsteady surface pressure as well as velocity measurements close to the surface of the plate. The link between the surface pressure at different points is examined to gain more insight on the surface pressure fluctuation and possible radiation of noise. The far field noise is then presented to show the effect of bevel angle on the radiated noise through the beamforming microphone array results.

A. Hydrodynamic Field

To gain an insight on the hydrodynamic field around the beveled trailing edge the pressure measurements are required to give an indication of the velocity field over the geometry and how the bevel angle affects this. Figure 2 presents the results of non-dimensional pressure coefficient and pressure fluctuations on the left and the right hand side of the figure respectively. The C_p and $C_{p_{rms}}$ values were calculated as,

$$C_{p_i} = \frac{\bar{p} - p_i}{p_{dyn}}, \tag{1}$$

$$C_{p_i,rms} = \frac{\sqrt{\sum_{i=1}^{N}(p_k - \bar{p})^2/N}}{p_{dyn}}, \tag{2}$$

where p_i is the ith data measured and p_k is the time sample measured, $\bar{p'}$ refers to the averaged pressure over the entire measurement duration, and the dynamic pressure p_{dyn} was calculated based on free stream velocity.

Considering the C_p distribution on the left hand side, the peak C_p value increases as the bevel angle increases. The first value upstream of the bevel shows relatively systematic increase of C_p with angle, $\alpha = 0^\circ$ having the lowest value and $\alpha = 26^\circ$ the highest value. The gap is the hinge point, and leading up to this point the pressure coefficient increases in all cases, but with a greater bevel angle comes an increasing gradient. The first measuring station after the hinge is the first station on the bevel and the location of the C_p maxima for all bevel angles, α, which then converges to a similar value at the trailing-edge. However, the pressure fluctuations C_{prms} do not follow the same trend as for C_p. The fluctuation level upstream of the bevel do not significantly vary for all angles, with only a small measured increase leading up to the hinge point. Once the bevel is reached, the fluctuation level dramatically increases for angles over $\alpha = 14^\circ$ and below this a fairly uniform behaviour is exhibited. The level of fluctuation increases from $\alpha = 14^\circ$ up to a maxima for $\alpha = 20^\circ$, for angles above this, the fluctuation returns to a level comparable to angles below $\alpha = 14^\circ$, with the exception of $\alpha = 28^\circ$.

To gain more insight on the behaviour shown by the hydrodynamic field and to better understand the flow behaviour over the flat plate and bevel, velocity profiles for $\alpha = 0^\circ$ and $\alpha = 28^\circ$ are demonstrated in Figure 3 on the left and right hand-side respectively. The velocity profiles measured at microphone location 1 and 11 is very similar for $\alpha = 0^\circ$, a behaviour typical of a boundary layer on a flat plate. At $\alpha = 28^\circ$, the velocity profile at $x'/l = 0.15$ suggests the flow is separated at the trailing-edge, represented by the hump between $y/H = 0$ and $y/H = 0.1$ which advocates a reversed flow and is induced by directional insensitivity of the single-wire probe and apparently represents negative velocity

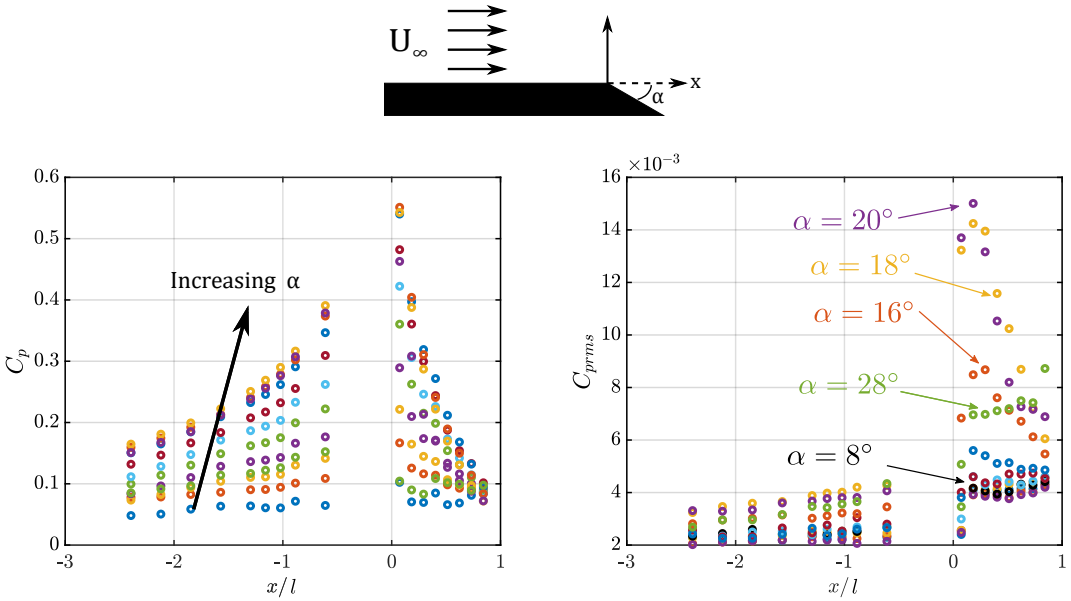

Fig. 2 C_p **(left) and** C_{prms} **(right) distribution over the flat plate for bevel angles** $0° < \alpha < 28°$

values. The large shear, visible between $y/H = 0.1$ and $y/H = 0.15$ signifies the separation. These boundary layer measurements exhibit behaviour that promotes the existence of a flow separation between $\alpha = 0°$ and $\alpha = 28°$ which will inherently affect the noise generation.

B. Near-field Structures

The velocity measurements of the flow over the bevel give an indication of the velocity field and steady mean flow characteristic of the boundary layer. To further understand and characterise the flow structures over the beveled trailing-edge the unsteady pressure fluctuation is assessed. The power spectral density (PSD) of the pressure fluctuations at each microphone locations are calculated as

$$\phi_{pp}(f) = 10 \log_{10} \left(\frac{\overline{p}'}{\overline{p}_{ref}} \right)^2, \tag{3}$$

where $\bar{p}'$ refers to the averaged pressure fluctuations and $p_{ref} = 20\mu Pa$ is the reference pressure. $\bar{p}'$ is obtained by converting the power spectral density of the measured signal at each microphone to pressure. Figure 4 demonstrates the comparison of PSD values at two different microphone locations at the hinge, at $x'/l = 1.42$, and the trailing edge, $x'/l = 0.15$, left and right, for bevel angles $\alpha = 0°$, $8°$, $18°$, $20°$ and $28°$. Displayed earlier in the velocity profiles the flow at $\alpha = 28°$ shows evidence of separated flow and PSD of the pressure fluctuation at both locations support this observation with a large decrease in the high frequency content of the fluctuation coupled with the increase of low frequency. Further alluding to presence of a large, separated structure. Between the two microphone locations, it is evident is that the overall energy content is higher closer to the bevel than at the trailing edge, although the overall trend remains the same. As the angle increases the low frequency content rises and the high frequency decreases, which is displayed to be consistent between the bevel location and the trailing edge. At the location of $x'/l = 1.42$, both $\alpha = 0°$ and $\alpha = 8°$ show a consistent energy level from low frequency to 1000 Hz where it begins to decay at higher frequencies. Increasing the bevel angle leads to the value of consistent energy inflation, but the turning point occurs at a lower frequency. The variation between the angles appears to be systematic changes in energy level and turning point up to $\alpha = 20°$. For the angle of $\alpha = 28°$, a steep decay is evident from 100 Hz, below which displays little change, this behaviour appears to be very different to the other angles displayed and hints at a complete change in flow structure. This behaviour is echoed by the signal at $x'/l = 0.15$ but the overall magnitude is approximately reduced by a consistent 10-15 dB.

The surface pressure fluctuation gives insight into the energy content of the flow at multiple locations along the bevel up to the trailing edge. To gain further insight on the coherent structures within the flow over the bevel the stream-wise

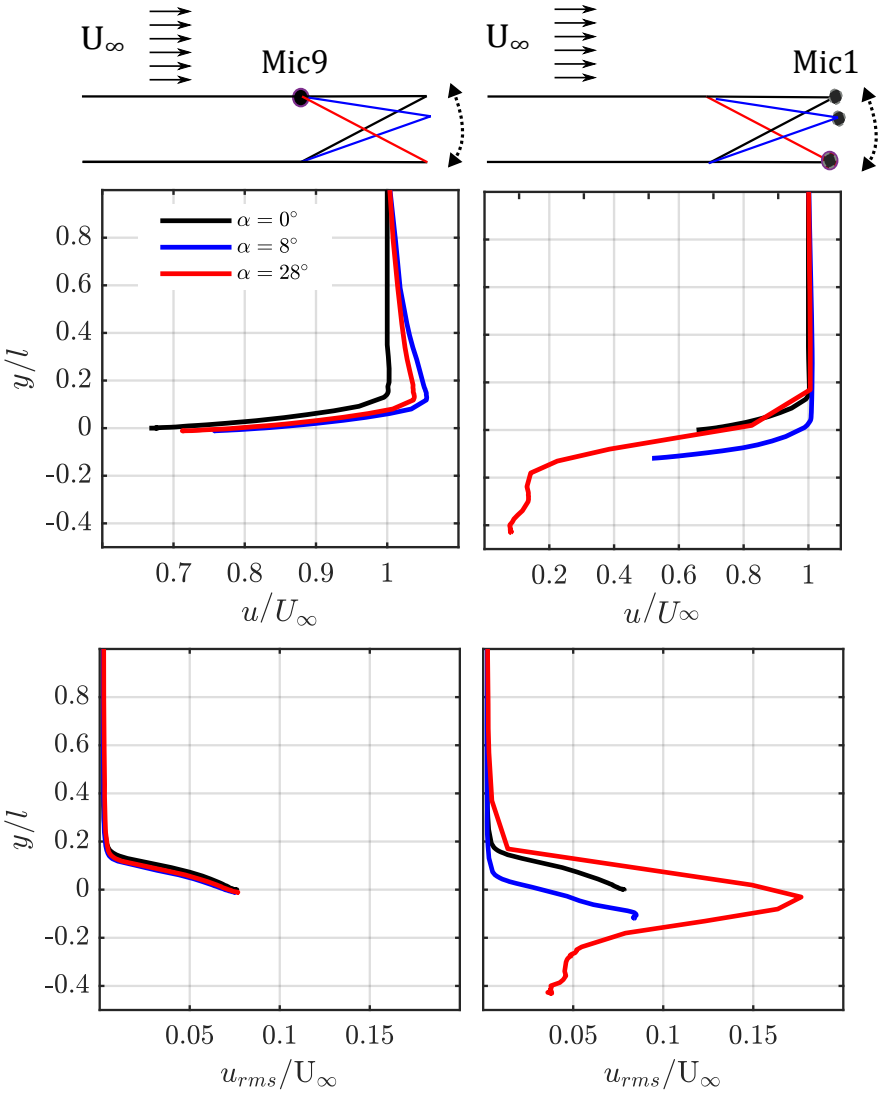

Fig. 3 Velocity profiles over microphone locations 1 and 9 at bevel angle $\alpha = 0°$ deg and $\alpha = 28°$

and span-wise coherence and the associated length scales are widely used tools to study this. The coherence was calculated as

$$\gamma^2_{p'_i p'_j} = \frac{\left|\phi_{p'_i p'_j}\right|^2}{\left|\phi_{p'_i p'_i}\right|\left|\phi_{p'_j p'_j}\right|}, \tag{4}$$

where $\gamma^2_{p'_i p'_j}$ is the span-wise coherence calculated between two microphones as i and j, and $\phi_{p'_i p'_j}$ is the cross-power spectral density.

Figure 5 is presented to demonstrate the stream-wise coherence of structures over the trailing edge for bevel angles $\alpha = 0°, 8°, 14°, 18°, 20°$ and $\alpha = 28°$. The microphones, which were used to calculate coherence with respect to reference microphone ($x'/l = 0.15$), are colour-coded and the same colour-code is also implemented in the graphs to ease the interpretation. For the case of the straight trailing edge, $\alpha = 0°$, the streamwise coherence of the upstream microphones reduces as the distance to the trailing edge decreases. A level of coherence, approximately 0.5 is seen for the closest microphone and it peaks between 150 and 300 Hz. Moving upstream away from the trailing edge the trend remains consistent, however the magnitude of the coherence decreases. Up to the hinge point and the furthest microphone from

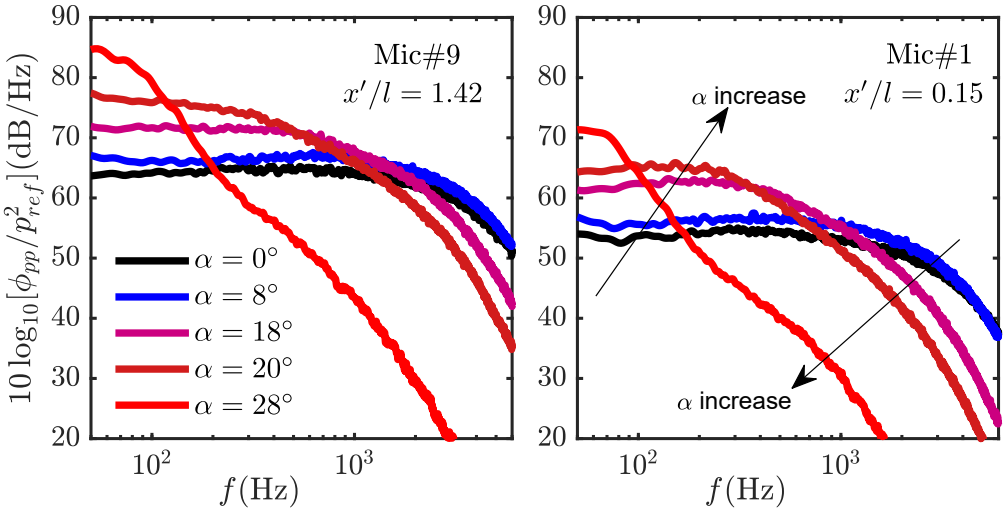

Fig. 4 Comparison of power spectral density of pressure fluctuations for bevel angles $0° < \alpha < 28°$ at microphone locations 1, $x'/l = 0.15$ and 9, $x'/l = 1.42$

the trailing edge where little coherence is shown to the trailing edge microphone. As the bevel increases to $\alpha = 8°$ the overall trend remains the same although the magnitude of coherence reduces and coherence between the upstream microphones is lost closer to the trailing edge. At a bevel angles of $\alpha = 14°$ and $\alpha = 18°$ the trend is comparable, likewise with $\alpha = 8°$, however the range of frequencies that coherence is seen for reduces as the angle increases, and the peak shifts to a lower frequency with a small increase in coherence magnitude. At $\alpha = 20°$ the peak coherence increases in magnitude but the effective peak frequency reduces to 100 Hz, and the range of coherence reduces further with exception to the introduction of coherence at low frequencies below 100 Hz a short distance upstream from the trailing edge. At a bevel angle of $\alpha = 28°$ the largest value of coherence is reported at a much lower frequency compared to the lower angles of α. This low frequency coherence is a further indicator of the separated flow in the region. There is also an increase in coherence at high frequency that should be investigated further.

To further characterise the flow within the turbulent boundary layer the time scales of the coherent structures were determined from an auto-correlation of the surface pressure fluctuations. The effect of the bevel angle on the auto-correlation of the surface pressure fluctuations is defined as,

$$R_{p_i' p_i'}(\tau) = \frac{\overline{p_i'(x_i, t+\tau) p_i'(x_i, t)}}{p'^2_{x_{irms}}}, \tag{5}$$

where p_i' is the wall pressure signal from the transducer located at x_i, $p_{x_{irms}}$ is the root-mean-square of the pressure fluctuation p_i' and τ represents the time delay between the signals. Figure 8 demonstrates $R_{p_i' p_i'}(\tau)$ for two microphone locations, $x'/l = 1.42$ and 1. Where the microphone at location $x'/l = 1.42$ is the microphone after the hinge and the microphone at location $x'/l = 0.15$ is the closest to the trailing edge, for various bevel angles between $\alpha = 0°$ and 28°. Auto-correlation analysis of the surface pressure fluctuation can give information about the largest scale of turbulence in the flow. On first inspection, two very different behaviours between the two positions at all angles above $\alpha = 8°$ is evident. At the $x'/l = 1.42$ location, a relatively uniform behaviour is seen for all angles, demonstrated by the collapse of the lines. Suggesting that at this point, bevel angle has little influence on the large scale structures in the flow. This trend continues to the trailing edge for angles below $\alpha = 8°$, the right hand side of Fig. 8 shows very similar behaviour between $\alpha = 0°$ and $\alpha = 8°$. Alternatively, $x'/l = 0.15$ at the trailing edge shows a very different behaviour for angles above $\alpha = 8°$. With increasing angle, the width of the auto-correlation function increases with the formation of a dominant negative correlation region in the function. This can be linked to evidence of the streamwise convection of spanwise vorticity [31], which can be interpreted as the shedding of large scale structures, again suggesting the presence of flow separation at large angles of α.

Figure 7 presents the coherence between the velocity and surface pressure signals at microphone locations 1 and 11 for trailing-edge bevel angles of $\alpha = 0°, 8°$ and $\alpha = 28°$ from left to right. The coherence between the velocity and surface pressure is defined as,

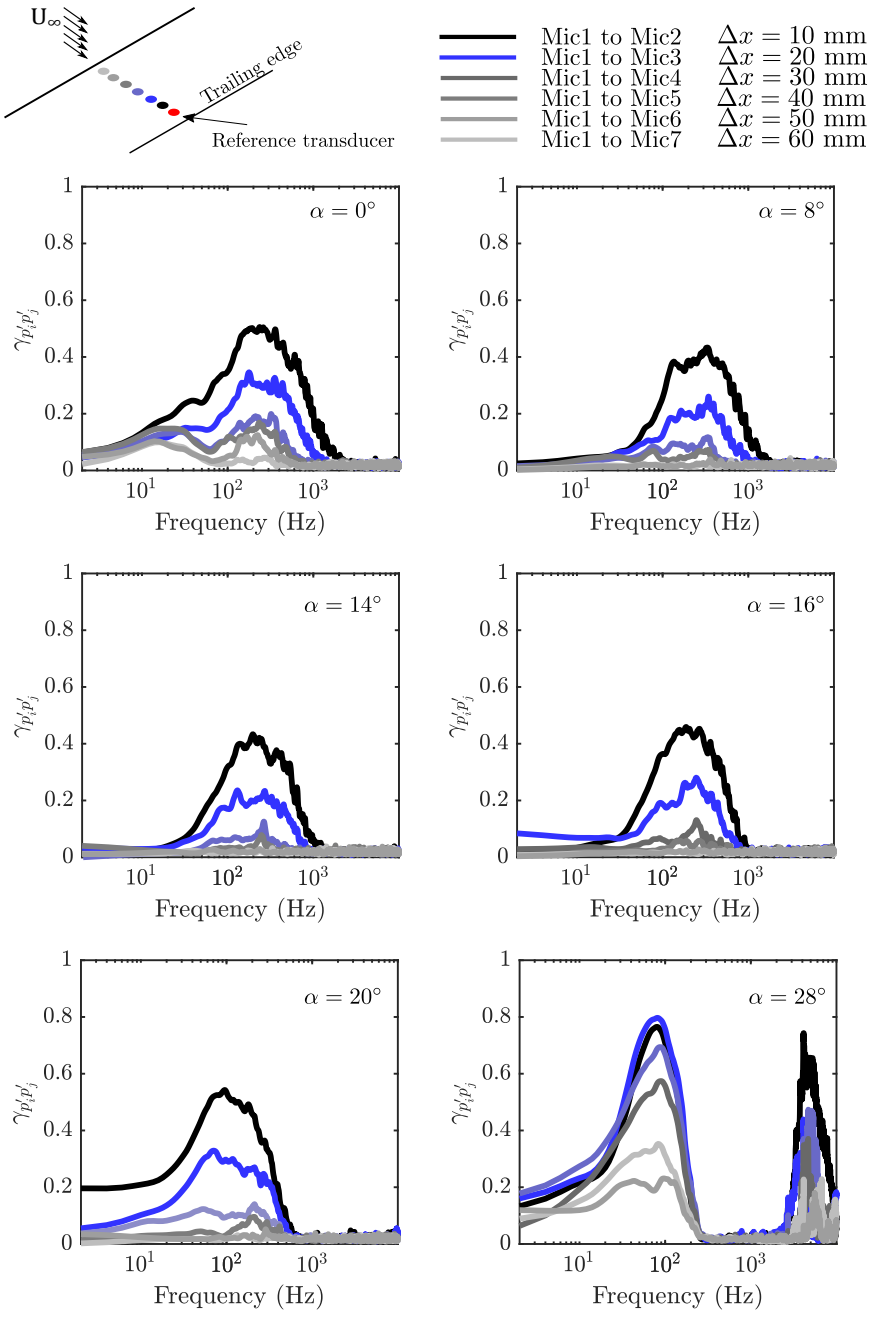

Fig. 5 Comparison of stream-wise $\gamma^2_{p'_i p'_j}$ for $0° < \alpha < 28°$

$$\gamma^2_{p'_i u'_i} = \frac{\left|\phi_{p'_i u'_i}\right|^2}{\left|\phi_{p'_i p'_i}\right|\left|\phi_{u'_i u'_i}\right|}, \tag{6}$$

where $\gamma^2_{p'_i u'_i}$ is the coherence calculated between the signal from corresponding microphone and velocity signal. $\phi_{p'_i p'_j}$ and $\phi_{u'_i u'_j}$ are the cross-power spectral density of pressure and velocity signal, respectively.

Considering the $\gamma^2_{p'_i u'_i}$ at $\alpha = 0°$, the coherence pattern is very similar for both microphones. Both exhibit coherence for the same range of frequencies and y distances, although at $x'/l = 0.15$ has a larger value of coherence over the

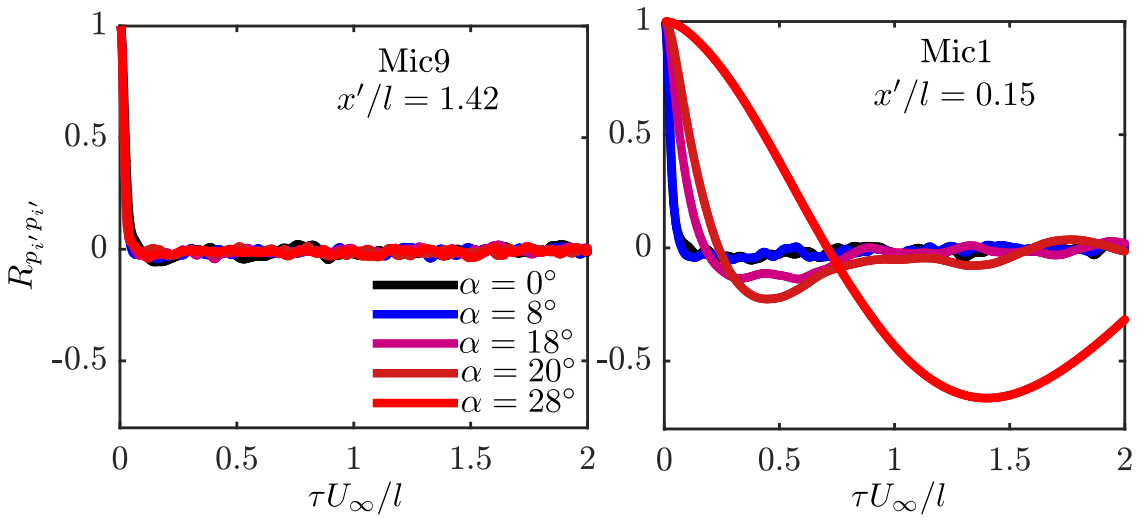

Fig. 6 Auto-correlation of surface pressure fluctuations $R_{p_i' p_i'}(\tau)$ at microphones 1 and 9 for bevel angles $\alpha = 0°, 8°, 18°, 20°$ and $28°$.

area. At a bevel angle $\alpha = 8°$ for location $x'/l = 1.42$, there is an increase in the range of frequencies and magnitude of coherence, as well as it's spacial spread compared to the $\alpha = 0°$ case. The coherence at location $x'/l = 0.15$ reduces in the overall level of coherence compared to both microphones for $\alpha = 0°$ and location $x'/l = 1.42$ for the same angle. When the separation occurs, at bevel angle $\alpha = 28°$, the coherence pattern at $x'/l = 1.42$ is very similar to $\alpha = 0°$. For $x'/l = 0.15$ a large region of very strong coherence is formed away from the surface of the bevel.

C. Far-field Noise

The far-field noise radiated from the trailing-edge of the flat plate was measured by an in-house built beamforming array to eliminate the contamination from the other possible sources such as side plates and nozzle. The data was collected for 120 seconds and presented in one-sixth octave band between 300 Hz and 3000 Hz. The data was averaged using time blocks of 4096 samples and windowed with a Hanning window of overlapping ratio of 50%. Figure 8 is constructed to demonstrate the effect of bevel angle on the far-field noise for a range of frequencies between 300 Hz and 3000 Hz. In order to better interpret the results and elaborate the effect of bevel angle, two subplots are presented within the figure. The left hand side displays the far field noise for angles $0° < \alpha < 8°$. The complicated nature in which the far field noise is emitted for the lower angles is shown by the collapse of the values on the spectra at lower and higher frequencies. At the highest and lowest frequencies that were measured the difference in the noise emitted between the angles is low. Over all the frequency range presented, the increase in bevel angle increases the radiated noise, and the increase becomes more apparent as the frequency increases, with the largest increase seen at 2000 Hz. Between 1000 Hz and 2000 Hz, as the frequency increases a plateau in the frequency spectral shape appears, but beyond 2000 Hz this collapses quickly to a similar noise level for all angles. Beyond $\alpha = 8°$ further increase in the bevel angle shifts the trend to a decreasing one, which presented in the lower right hand figure by far field noise across $10° < \alpha < 28°$. At a bevel angle of $\alpha = 10°$, the radiated noise is less than that of the $\alpha = 8°$ case, and it continues to reduce as the bevel angle increases, and again the difference appears to grow larger at higher frequencies. Considering the bevel angle beyond 18°, where a fully separated flow is experienced, which was displayed by the flow field analysis, the bevelled trailing edge radiates even less noise compared to a flat plate. At an angle of $\alpha = 8°$, there is a turning point where the noise generated by the flow peaks. Full separation noise is lower than that off the flat plate case due to the convected eddies in the shear layer no longer interacting with the trailing edge, which is the suggested reason for the reduction in noise for the $\alpha = 28°$ case.

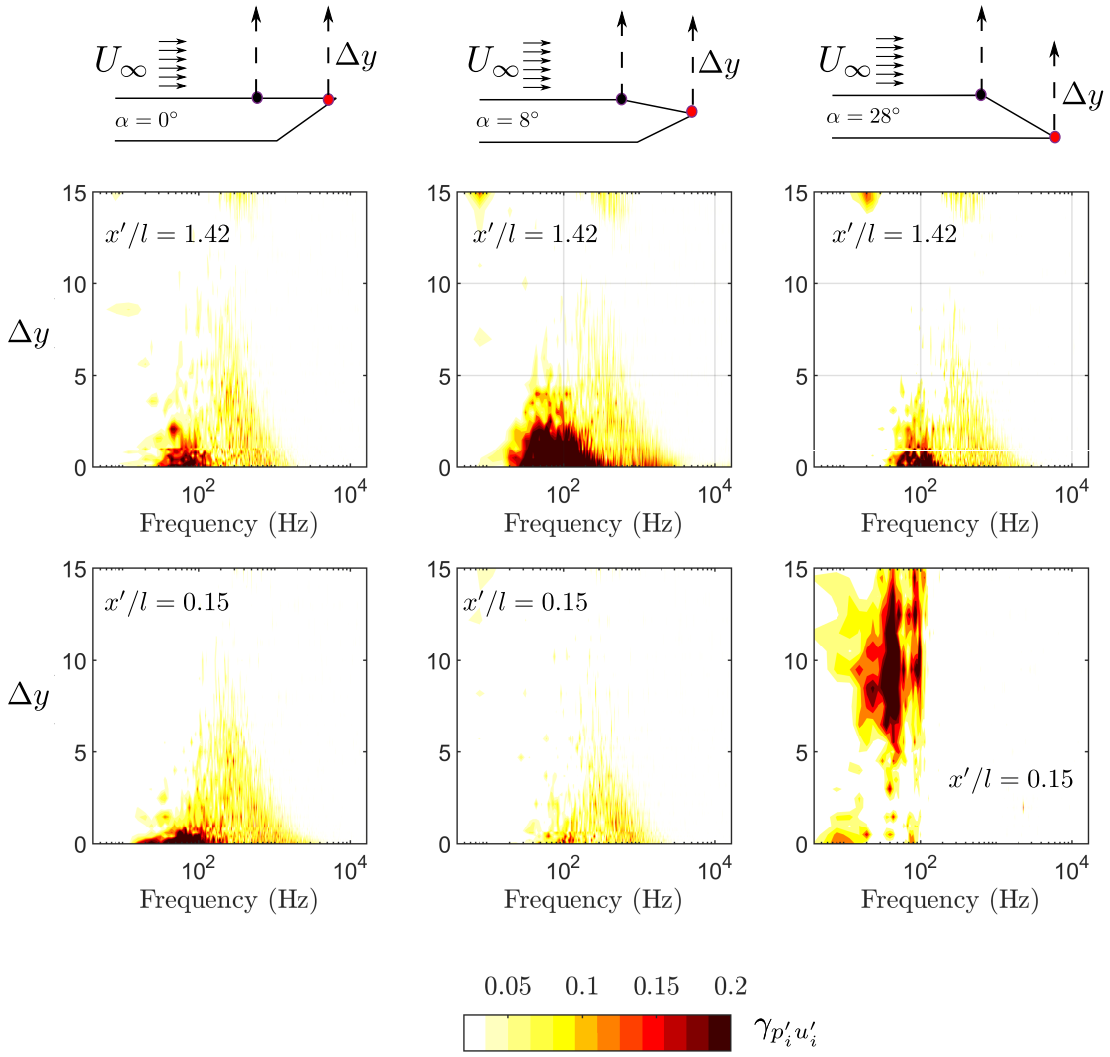

Fig. 7 Velocity-pressure coherence $\gamma^2_{p'_i u'_i}$ for microphone locations 1 and 11 for bevel angles $\alpha = 0°, 8°$ and $\alpha = 28°$.

V. Conclusion

This paper provides an extensive study to understand the effect of bevel angle on the noise generated flow past a trailing edge and its hydrodynamic field. A flat plate test rig was designed, manufactured and tested to investigate the effect of trailing-edge bevel angle on the radiated noise and its corresponding flow field. For the tested configuration, the results show that an increase in bevel angle increases the radiated noise up to a critical angle. Further increase in the bevel angle leads a change in the trend and the radiated noise starts to decrease. The flow field analysis shows that beyond a certain angle the flow around the beveled trailing edge becomes fully separated, which is a suggested cause for the change in the noise emission. In this case a bevel angle of $\alpha = 8°$ shows the greatest noise emission when compared to a flat plate although further study is required to identify the specific cause of the increase at this angle.

Acknowledgments

The authors would like thank Dr. Bin Zang for his valuable contribution in beamforming analysis and Dr. Xiao Liu for her valuable contributions in manufacturing the rig.

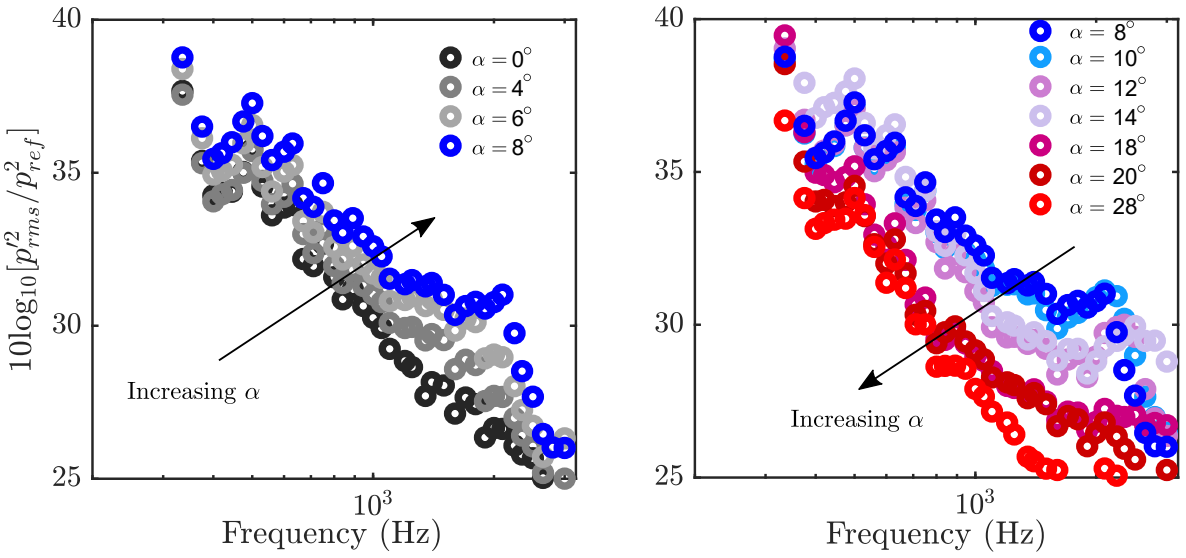

Fig. 8 Beamforming results for trailing edge bevel angle $0^\circ < \alpha < 8^\circ$ (left) and $8^\circ < \alpha < 28^\circ$(right).

References

[1] Brooks, T., Pope, D., and Marcolini, M., "Airfoil self-noise and prediction," Tech. rep., National Aeronautics of Space Administration, Office of Management, 1989.

[2] Amiet, R. K., "Noise due to turbulent flow past a trailing edge," *Journal of sound and vibration*, Vol. 47, No. 3, 1976, pp. 387–393.

[3] Williams, J. E. F., and Hall, L. H., "Aerodynamic sound generation by turbulent flow in the vicinity of a scattering half plane," *Journal of Fluid Mechanics*, Vol. 40, No. 4, 1970, p. 657–670. https://doi.org/10.1017/S0022112070000368.

[4] Howe, M., "The influence of surface rounding on trailing edge noise," *Journal of Sound and Vibration*, Vol. 126, No. 3, 1988, pp. 503 – 523. https://doi.org/https://doi.org/10.1016/0022-460X(88)90227-1.

[5] Szoke, M., and Azarpeyvand, M., "Active Flow Control Methods for the Reduction of Trailing Edge Noise," Proceedings of the 23rd AIAA/CEAS Aeroacoustics Conference, Denver, CO, AIAA 2017-3004.

[6] Szőke, M., Fiscaletti, D., and Azarpeyvand, M., "Effect of inclined transverse jets on trailing-edge noise generation," *Physics of Fluids*, Vol. 30, No. 8, 2018, p. 085110.

[7] Showkat Ali, S., Azarpeyvand, M., and Ilário da Silva, C., "Trailing-edge flow and noise control using porous treatments," *Journal of Fluid Mechanics*, Vol. 850, 2018, p. 83–119.

[8] Mayer, Y. D., Lyu, B., Jawahar, H. K., and Azarpeyvand, M., "A semi-analytical noise prediction model for airfoils with serrated trailing edges," *Renewable Energy*, Vol. 143, 2019, pp. 679 – 691. https://doi.org/https://doi.org/10.1016/j.renene.2019.04.132.

[9] Liu, X., Jawahar, H. K., Azarpeyvand, M., and Theunissen, R., "Aerodynamic Performance and Wake Development of Airfoils with Serrated Trailing-Edges," *AIAA Journal*, Vol. 55, No. 11, 2017, pp. 3669–3680.

[10] Lyu, B., and Azarpeyvand, M., "On the noise prediction for serrated leading edges," *Journal of Fluid Mechanics*, Vol. 826, 2017, p. 205–234.

[11] Avallone, F., Pröbsting, S., and Ragni, D., "Three-dimensional flow field over a trailing-edge serration and implications on broadband noise," *Physics of Fluids*, Vol. 28, No. 11, 2016, p. 117101.

[12] Ragni, D., Avallone, F., van der Velden, W., and Casalino, D., "Measurements of near-wall pressure fluctuations for trailing-edge serrations and slits," *Experiments in Fluids*, Vol. 60, No. 1, 2018, p. 6.

[13] Jawahar, H. K., Ai, Q., and Azarpeyvand, M., "Experimental and numerical investigation of aerodynamic performance for airfoils with morphed trailing edges," *Renewable Energy*, Vol. 127, 2018, pp. 355 – 367. https://doi.org/https://doi.org/10.1016/j.renene.2018.04.066.

[14] Jawahar, H. K., Theunissen, R., Azarpeyvand, M., and da Silva, C. R. I., "Flow characteristics of slat cove fillers," *Aerospace Science and Technology*, Vol. 100, 2020, p. 105789. https://doi.org/https://doi.org/10.1016/j.ast.2020.105789, URL http://www.sciencedirect.com/science/article/pii/S1270963819321261.

[15] Jawahar, H. K., Ali, S. A. S., Azarpeyvand, M., and da Silva, C. R. I., "Aerodynamic and aeroacoustic performance of high-lift airfoil fitted with slat cove fillers," *Journal of Sound and Vibration*, 2020, p. 115347. https://doi.org/https://doi.org/10.1016/j.jsv.2020.115347.

[16] Herr, M., and Dobrzynski, W., "Experimental Investigations in Low-Noise Trailing Edge Design," *AIAA Journal*, Vol. 43, No. 6, 2013, pp. 1167–1175.

[17] Chong, T., and Vathylakis, A., "On the aeroacoustic and flow structures developed on a flat plate with a serrated sawtooth trailing edge," *Journal of Sound and Vibration*, Vol. 354, 2015, pp. 65 – 90.

[18] Catlett, M. R., Devenport, W., and Glegg, S. A., "Sound from boundary layer flow over steps and gaps," *Journal of Sound and Vibration*, Vol. 333, No. 18, 2014, pp. 4170 – 4186. https://doi.org/https://doi.org/10.1016/j.jsv.2014.03.042.

[19] Camussi, R., Guj, G., and Ragni, A., "Wall pressure fluctuations induced by turbulent boundary layers over surface discontinuities," *Journal of Sound and Vibration*, Vol. 294, No. 1, 2006, pp. 177 – 204. https://doi.org/https://doi.org/10.1016/j.jsv.2005.11.007.

[20] Blake, W. K., "A Statistical Description of Pressure and Velocity Fields at the Trailing Edges of a Flat Strut," Tech. rep., David W. Taylor Naval Ship Research and Development Center,, 1975.

[21] Blake, W. K., "Trailing Edge Flow and Aerodynamic Sound," Tech. Rep. DTNSRDC-83/113, David W. Taylor Naval Ship Research and Development Center,, 1984.

[22] Howe, M., "Trailing Edge Noise at low Mach numbers," *Journal of Sound and Vibration*, Vol. 225, No. 2, 1999, pp. 211 – 238. https://doi.org/https://doi.org/10.1006/jsvi.1999.2236.

[23] Howe, M., "Trailing Edge Noise at low Mach numbers, PART 2: Attached and separated edge flows," *Journal of Sound and Vibration*, Vol. 234, No. 5, 2000, pp. 761 – 775. https://doi.org/https://doi.org/10.1006/jsvi.1999.2861.

[24] Bilka, M. S. C. B. C. S. J. C. S. D. W., M. J., "Flowfield and Sound from a Blunt Trailing Edge with Varied Thickness," *AIAA Journal*, Vol. 52, No. 1, 2014, pp. 52–61.

[25] Pronsting, G. A., S. and., Scarano, F., Guan, Y., and Morris, S., "Tomographic PIV for Beveled Trailing Edge Aeroacoustics," *AIAA AVIATION Forum 20th AIAA/CEAS Aeroacoustics Conference*, Vol. 52, No. 1, 2014, pp. 52–61.

[26] van der Velden, W., Pröbsting, S., van Zuijlen, A., de Jong, A., Guan, Y., and Morris, S., "Numerical and experimental investigation of a beveled trailing-edge flow field and noise emission," *Journal of Sound and Vibration*, Vol. 384, 2016, pp. 113 – 129. https://doi.org/https://doi.org/10.1016/j.jsv.2016.08.005, URL http://www.sciencedirect.com/science/article/pii/S0022460X16303935.

[27] Guan, Y., Pröbsting, S., and Morris, S. C., "Unsteady surface pressure characteristics of asymmetrically beveled trailing edges," *Experiments in Fluids*, Vol. 59, No. 7, 2018, p. 118. https://doi.org/10.1007/s00348-018-2572-6, URL https://doi.org/10.1007/s00348-018-2572-6.

[28] Guan, Y., Pröbsting, S., Morris, S. C., Stephens, D., and Morris, S. C., "On the wake flow of asymmetrically beveled trailing edgess," *Experiments in Fluids*, Vol. 57, No. 5, 2016, p. 78. https://doi.org/10.1007/s00348-016-2172-2.

[29] Mayer, Y., Jawahar, H., Szoke, M., and Azarpeyvand, M., "Design of an Aeroacoustic Wind Tunnel Facility at the University of Bristol," Proceedings of the 24th AIAA/CEAS Aeroacoustics Conference , Atlanta, GA, AIAA 2018-3138.

[30] Mayer, Y., Zang, B., and Azarpeyvand, M., *Design of a Kevlar-Walled Test Section with Dynamic Turntable and Aeroacoustic Investigation of an Oscillating Airfoil*, chapter and pages. https://doi.org/10.2514/6.2019-2464, URL https://arc.aiaa.org/doi/abs/10.2514/6.2019-2464.

[31] Glegg, S., and Devenport, W., *Aeroacoustics of low Mach number flows: fundamentals, analysis, and measurement*, Academic Press, 2017.